PHYSICAL REVIEW A VOLUME 18, NUMBER 5 NOVEMBER 1978

Projectile dependence of single-K multiple-L shell vacancy production in argon: A universal scaling of $\langle l \rangle$

Carl Schmiedekamp, B. L. Doyle, Tom J. Gray, R. K. Gardner, K. A. Jamison, and Patrick Richard
Department of Physics, Kansas State University, Manhattan, Kansas 66502
(Received 14 November 1977)

Argon $K\alpha$ x-ray satellites produced by ion collisions have been analyzed in high resolution. Ions of H, C, N, O, F, Si, and Cl with energies in the range 1–5 MeV/amu were used to bombard argon contained in a gas cell. This study is the first systematic study of K x-ray satellites from free-atom targets with $Z > 10$. The relative satellite intensities and satellite energies are tabulated and their projectile dependence is qualitatively discussed. The average number of L-shell vacancies formed in single-K-vacancy-producing collisions is determined from a model calculation based on theoretical decay rates. This model includes (i) the variation in fluorescence yield, and (ii) the variation in L-shell rearrangement with the number of L-shell and M-shell electrons. The averages obtained from the model calculation are nearly the same as the $\langle l \rangle$ values obtained by weighting the x-ray satellites equally. A universal scaling of $\langle l \rangle$ in Z_1 and projectile velocity is obtained on the basis of an increased binding effect. This is the first successful demonstration of a scaling law for multiple ionization by heavy ions.

I. INTRODUCTION

$K\alpha$ x-ray satellites from ion-atom collisions in solid targets have been studied for several years.[1-5] It has been shown that the distribution of L-shell vacancies which produces the $K\alpha L^n$ satellites can be fit to a binomial distribution in the probability for L-shell vacancy production at small impact parameters $P_L(0)$. These studies have been extended to gas targets where single-collision conditions are easier to satisfy.[6,7] In these two experiments using a Ne gas target, it was shown that the distribution of L-shell vacancies follows a binomial distribution as in the case of the solid targets, however, the distribution does depend on the charge state of the incident ion which can be maintained in the gas collision region. The $P_L(0)$ values increase with increasing charge state. In the solid target case the probability of L-shell ionization appears to saturate at values near 0.3, for low-Z targets as one increases the Z of the projectile in the 1–2-MeV/amu energy range, whereas L-shell vacancy probabilities as large as 0.65 have been observed in the gas target experiments.

Additional considerations to this problem have been presented in three recent experiments. Kauffman *et al.*[8] have shown that the $K\alpha$ satellite structure of SiH_4 differs substantially from that obtained with a thin solid Si target. The data implies that large L-shell decay rates are required in the solid to produce the L-shell rearrangement observed in the x-ray spectra, assuming that the KL^n ionization cross sections are the same in the solid as in the gas target. Watson *et al.*[3,9] have shown that the spectra of different compounds of S in solid targets display different $K\alpha L^n$ distributions which they have attributed to interatomic electron rearrangement. Hopkins *et al.*[10] have shown further that molecular gas targets yield different satellite distributions. Light ligand gases such as SiH_4 have a higher $K\alpha L^n$ centroid than does a heavy ligand gas such as SiF_4. The heavy ligand gases in fact display $K\alpha L^n$ spectra closely resembling the spectra of solid targets. A similar rearrangement mechanism must be leading to the qualitatively identical spectra observed in the solid, solid molecular, and gas molecular targets.

In the present paper we study the problem of multiple ionization in ion-atom collisions with a free atom target in which only *atomic* rearrangement is present. The transformation from deexcitation K x-ray satellite probabilities to vacancy formation probabilities still requires the consideration of variation of fluorescence yield with primary vacancy configurations and the rearrangement of the L-shell vacancies through intraatomic transitions. The only monoatomic gas studied[7] systematically is Ne which has the difficulties of a very small K-shell fluorescence yield for the characteristic line and therefore has a very large variation of fluorescence yield[11,12] with the number of L-shell vacancies. Ne also has a very small L-shell binding energy so that the L-shell ionization cross section is very sensitive to variations in the L-shell binding energies.

We present a systematic study of the Ar $K\alpha$ satellite formation in H, C, N, O, F, Si, and Cl bombardment in the energy range of 1–5 MeV/amu. Effects of L-shell rearrangement and fluorescence yield are taken into account by a model

calculation which utilizes the available theoretical decay rates[13-15] for Ar. The extracted L-shell ionization probabilities do not scale as $1/Z_1^2$ as predicted by Coulomb ionization theories.[16-19] The effects of including an increased binding factor ϵ is investigated. Semiempirical scalings of the form $P_L\epsilon/Z_1^2$ vs v/ϵ for the plane-wave Born approximation (PWBA) model and $P_L\epsilon^2/Z_1^2$ vs $v/\sqrt{\epsilon}$ for the binary-encounter approximation (BEA) model are studied. The effects of charge exchange are not included in the analysis and may well lead to better fits to the data.

II. PROCEDURE

The argon $K\alpha$ satellites ($K\alpha L^l$) were produced by bombardment of argon in a high pressure gas cell. This cell has an entrance window of 1-mg/cm^2 Ni foil. The beam stop is internal to the gas cell so no exit window for the beam is used. The exit window for the x rays is a 6-μm aluminum coated Mylar window.

The gas cell was filled to ~100 Torr of argon. Higher pressures degraded the beam quality for some of the beams before they reached the viewing region of the spectrometer. The viewing region was defined by an entrance slit to the spectrometer which also serves to support the Mylar window. The beam collimators and the beam stop were kept outside the viewing region of the spectrometer.

The x rays were analyzed with a 4-in. curved crystal spectrometer placed 90° to the beam axis. The spectrometer used a NaCl crystal ($2d=5.641$ Å). The data for all spectra were taken in a multiscalar mode and most spectra were repeated to check reproducibility.

The beam stop could not be used as an accurate monitor of the ion beam because of its location in the gas and because of its small size. Instead a proportional counter was mounted on the opposite side of the beam from the spectrometer. This detector has an adjustable entrance aperture. This monitor provided a good indication of beam intensity variations but had gas density dependence due to the absorption of the x rays by the argon gas. To prevent density changes the gas cell was closed off from the filling system during the collection of a spectrum.

III. THEORY

The experimental quantities obtained from the $K\alpha L^l$ satellite spectra are $\langle l\rangle$, the average L-shell satellite number, and ΔE_l, the energy shift of the $K\alpha L^l$ satellite peaks. These two quantities can be used to determine the probability of L-shell ionization at zero impact parameter $P_L(0)$. In the lowest order $P_l(0)=\frac{1}{8}\langle l\rangle$. This approximation assumes that the vacancy production for the $K\alpha L^l$ states follows a binomial distribution, that the transitions from these states have equal fluorescence yields, and that there is no outer-shell rearrangement prior to filling of the K shell. In a second method the variation of fluorescence yield with the number of L-shell and M-shell vacancies is taken into account as well as the effects of outer-shell rearrangement due to L-MM Auger transitions.

The second method attempts to estimate $\langle l\rangle$ and the energy shifts of the satellites by using binomial statistics for the production of the vacancies and tabulated and estimated fluorescence yields of the appropriate defect configurations. The model has as its input parameters the probability for producing an L-shell vacancy P_L and the probability for producing an M-shell vacancy P_M. These effective probabilities may include all mechanisms for vacancy production, not direct Coulomb ionization alone. From these parameters an initial vacancy matrix is constructed with the element corresponding to l L-shell vacancies and m M-shell vacancies given by

$$V^I(l,m)=\binom{8}{l}P_L^l(1-P_L)^{8-l}\binom{8}{m}P_M^m(1-P_M)^{8-m}. \tag{1}$$

Rearrangement is then permitted via L-MM Auger transitions. This is accomplished by calculating a new matrix of vacancies with the expression

$$\begin{aligned}V^R(l,m)&=V^I(l,m)\\&\quad+F_{l-1,m+2}[V^I(l-1,m+2)\\&\qquad+F_{l-2,m+4}(V^I(l-2,m+4)+\cdots)],\end{aligned} \tag{2}$$

where $F_{i,j}$ is the ratio of the L-MM Auger rate to the total decay rate for a vacancy configuration of i L-shell vacancies and j M-shell vacancies. The rates used are averaged over subshells, and the L-shell vacancies filled by the L-MM transitions are assumed to be evenly divided among the L subshells. The L-Auger rates used were obtained from McGuire[20] with Larkins scaling[21] for M- and L-shell vacancies. The K-shell rates were obtained from the tables of Bhalla[14] with smoothly extrapolated values used for configurations not given.

The relative satellite intensity for l L-shell and m M-shell vacancies is then given by

$$I(l,m)=\omega_K(l,m)V^R(l,m), \tag{3}$$

where $\omega_K(l,m)$ is the fluorescence yield for a $K\alpha$ transition with l L-shell vacancies and m M-shell

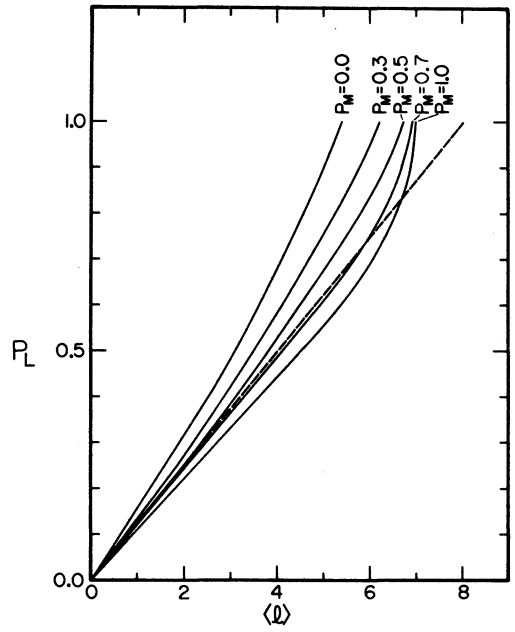

FIG. 1. Model predictions of argon $K\alpha L^l$ average satellite number $\langle l\rangle$. P_L and P_M are one-electron vacancy-production probabilities for the L shell and M shell, respectively. The dashed line corresponds to $\langle l\rangle = 8P_L$.

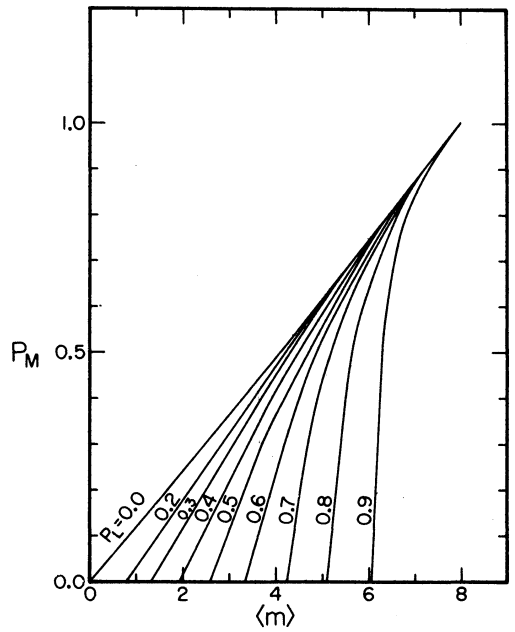

FIG. 2. Model predictions of the average number of M-shell vacancies in argon. P_L and P_M are one-electron vacancy production probabilities for the L shell and M shell, respectively.

vacancies.

The calculated $\langle l\rangle$ is then obtained from the expression

$$\langle l\rangle = \Big[\sum_{l=0}^{7} l\Big(\sum_{m=0}^{8} I_{l,m}\Big)\Big] \Big/ \Big(\sum_{l=0}^{7}\sum_{m=0}^{8} I_{l,m}\Big), \quad (4)$$

where $I_{l,m}$ are the matrix elements of the matrix $I(l,m)$. The average effective M-shell vacancy for the $K\alpha L^l$ satellite is obtained from the expression

$$\langle m\rangle_l = \Big(\sum_{m=0}^{8} mI_{l,m}\Big) \Big/ \Big(\sum_{m=0}^{8} I_{l,m}\Big). \quad (5)$$

This quantity $\langle m\rangle_l$, is related to the energy shifts ΔE_l of the $K\alpha L^l$ satellites.[14]

This model was used to investigate the effect of M-shell vacancies on the observed satellite distribution. Figure 1 shows several curves calculated for different values of the M-shell vacancy production probability P_M. The centroid of the spectrum $\langle l\rangle$ is predicted to change by as much as 30% depending on the value of P_M or on the average number of M-shell vacancies. The relative change in $\langle l\rangle$ with P_M is seen to be almost independent of P_L, the probability per electron of producing an L-shell vacancy. The straight line is the prediction given by the first approximation $[P_L(0) = \frac{1}{8}\langle l\rangle]$, as discussed above. The large variation of P_L in the rearrangement model from the $\frac{1}{8}\langle l\rangle$ line is for the unlikely event of large L-shell vacancy production with small M-shell vacancy production.

Figure 2 shows a similar set of curves for the effective average number of M-shell vacancies $\langle m\rangle$. This figure indicates that the number of M-shell vacancies is a strong function of the number of initial L-shell vacancies when P_M is small. As P_M increases, the variation in $\langle m\rangle$ due to rearrangement becomes smaller, so that in the case of Ar this model predicts a large rearrangement in the case of small P_M and large P_L.

This two-parameter model can be used by an iterative process to obtain estimates of P_L and P_M, given the measured $\langle l\rangle$ and $\langle m\rangle$ values.

IV. EXPERIMENTAL RESULTS AND ANALYSIS

A. Semiempirical analysis

Representative spectra for 1.9- or 1.95-MeV/amu ions are shown in Fig. 3. From each spectrum the energies of the satellites and the average L-shell satellite number $\langle l\rangle$ were obtained. Tables I and II list the satellite energies and the average L-shell satellite number $\langle l\rangle$. Experimentally $\langle l\rangle$ is defined by the expression

$$\langle l\rangle = \Big(\sum_{n=0}^{7} nI_n\Big) \Big/ \Big(\sum_{n=0}^{7} I_n\Big), \quad (6)$$

where I_n are the measured x-ray satellite intensities.[6] The quantity $\langle l\rangle$ is a measure of the num-

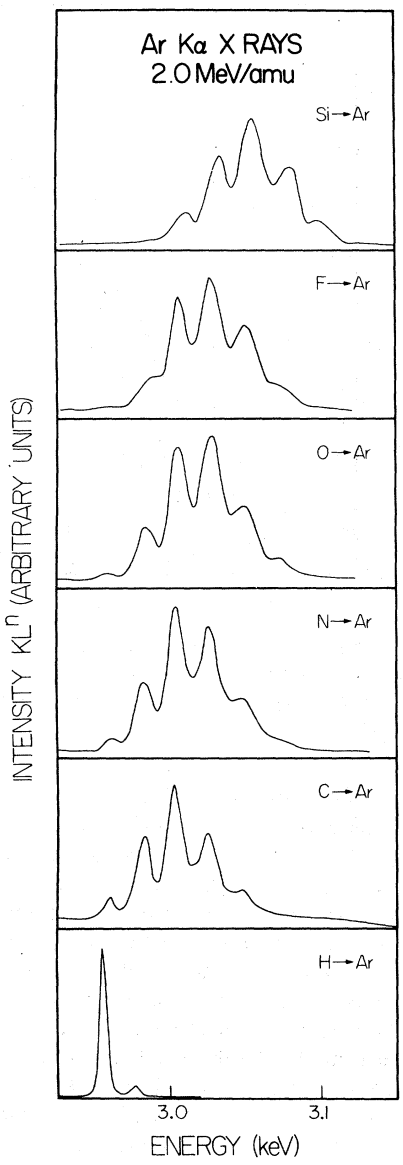

FIG. 3. Representative spectra for 2-MeV/amu ions incident on argon. Due to energy loss in the gas cell windows the collision energies are 1.9 MeV/amu for H ions and 1.95 MeV/amu for Si, F, O, N, and C ions.

ber of L-shell vacancies at the time of the $K\alpha$ transition.

In the semiempirical analysis presented in this section we assume that the observed average L-shell satellite number is proportional to the probability of L-shell ionization. This assumption is valid when the effects of vacancy rearrangement, vacancy-dependent K-fluorescence yields, and vacancy production by electron transfer are small.

Over the rather small energy range of the data the $\langle l \rangle$ tends to vary linearly with the velocity squared (E/A) of the ion and to have a strong dependence on the atomic number of the projectile (Z_1) as can be seen in Fig. 4. The Z_1 dependence is partially described by a $1/Z^2$ scaling as would be predicted by a simple binary encounter (BEA)[18] or plane-wave Born approximation[17] for direct Coulomb ionization. Figure 5 depicts the scaled results.

In anticipation that the remaining Z_1 dependence could be described as an increased binding of the L-shell electrons, the data were fit to BEA and PWBA ionization curves.[18,19] The data were scaled with a parametrized binding correction factor ϵ. The scaling was obtained by a least-squares fit of the $\langle l \rangle$ to a scaled universal ionization function of the form

$$Kf(V\epsilon^{-\mu})Z_1^2\epsilon^{-\nu}, \tag{7}$$

where K is a proportionality constant, $f(V\epsilon^{-\mu})$ is the ionization function, V is the scaled velocity of the incident ion relative to the L-shell electron velocity, and ϵ is the binding correction factor. Two sets of values for μ and ν were used. The PWBA theory predicts that μ and ν should both be 1 while the BEA theory predicts that μ should be 0.5 and ν should be 2. The correction factor ϵ is defined by the equation $U_c = \epsilon U_B$, where U_c is the "corrected" binding energy, and U_B is the normal, unperturbed binding energy. For U_B we have used the binding energy of the $L2$ subshell of argon. Several methods have been suggested for

TABLE I. (A) Energy shifts in argon $K\alpha$ L^l satellites[a].

	ΔE (eV)				
Z_1	$K\alpha\, L^0$	$K\alpha\, L^1$	$K\alpha\, L^2$	$K\alpha\, L^3$	$K\alpha\, L^4$
1	0.5	1.07	...	...	...
6	4.4	5.8	6.0	7.3	8.8
7	4.7	6.7	6.5	8.2	11.2
8	5.2	7.6	7.9	9.8	12.7
9	5.9	9.2	8.8	10.8	13.4
14	...	13.0	13.0	13.9	16.8
17	...	12.5	12.6	14.9	18.0

(B) Extrapolated satellite positions

Satellite	Channel	λ (Å)	E (eV)
$K\alpha\, L^0$	34.88	4.1928[b]	2956
$K\alpha\, L^1$	57.60	4.166	2976
$K\alpha\, L^2$	82.41	4.137	2997
$K\alpha\, L^3$	106.11	4.109	3017
$K\alpha\, L^4$	128.59	4.083	3036
$K\alpha\, L^5$	163.19	4.042	3067

[a] Energies are relative to an extrapolated energy at $Z=0$. The relative error is ~1.0 eV in the energy shift.
[b] Taken as energy calibration point.

TABLE II. L-shell and M-shell vacancy probabilities obtained under the different assumptions discussed in text.

Z Proj.	E (MeV/amu)	P_L [a] $=\frac{1}{8}\langle l\rangle$	P_L With Rearrangement	P_M With Rearrangement	P_L Without Rearrangement	P_M Without Rearrangement
1	0.85	0.015(4)	0.017	0.09	0.017	0.10
	1.38	0.013(4)	0.016	0.09	0.016	0.10
	1.64	0.010(3)	0.011	0.09	0.011	0.10
	1.90	0.010(2)	0.011	0.09	0.011	0.10
	2.16	0.010(3)	0.011	0.09	0.011	0.10
	2.41	0.010(2)	0.009	0.09	0.009	0.10
	2.67	0.008(2)	0.009	0.09	0.009	0.10
	2.92	0.008(2)	0.009	0.09	0.009	0.10
	3.94	0.006(2)	0.006	0.09	0.006	0.10
	4.95	0.006(2)	0.007	0.09	0.007	0.10
6	1.44	0.30 (4)	0.31	0.41	0.30	0.46
	1.70	0.29 (4)	0.30	0.41	0.30	0.46
	1.95	0.28 (4)	0.29	0.42	0.29	0.46
	2.20	0.26 (4)	0.27	0.42	0.26	0.46
	2.46	0.24 (3)	0.25	0.43	0.25	0.46
	2.71	0.23 (3)	0.24	0.43	0.23	0.46
	2.96	0.22 (3)	0.23	0.43	0.22	0.46
7	1.70	0.32 (4)	0.33	0.47	0.32	0.51
	1.95	0.31 (4)	0.32	0.47	0.31	0.51
	2.20	0.30 (4)	0.31	0.48	0.30	0.51
	2.46	0.29 (4)	0.30	0.48	0.29	0.51
8	1.70	0.34 (4)	0.35	0.53	0.34	0.56
	1.95	0.34 (4)	0.34	0.53	0.34	0.56
	2.20	0.33 (4)	0.34	0.53	0.33	0.56
	2.46	0.33 (4)	0.33	0.53	0.32	0.56
9	1.44	0.38 (5)	0.37	0.62	0.37	0.64
	1.70	0.38 (5)	0.38	0.62	0.37	0.64
	1.95	0.36 (4)	0.36	0.62	0.35	0.64
	2.20	0.36 (4)	0.35	0.62	0.35	0.64
	2.46	0.37 (4)	0.36	0.62	0.36	0.64
14	1.44	0.44 (7)	0.42	0.78	0.42	0.78
	1.70	0.47 (6)	0.44	0.78	0.44	0.78
	1.95	0.49 (6)	0.46	0.78	0.46	0.78
17	1.44	0.45 (6)	0.42	0.76	0.42	0.77

[a] This column is taken directly from the x-ray yields according to Eq. (6). Fluorescence yields are assumed independent of number of L-shell vacancies as discussed in text. The number in parenthesis is the experimental error in the last digit.

estimating the binding correction for ionization and electron capture which provide the correction in polynomial form. Several authors[22-24] have suggested using the form $\epsilon = 1 + (2Z_1/Z_{2L}\theta_L)g$ as the binding correction, where Z_{2L} is $Z_2 - 4.15$, θ_L is given by $4U_B/[Z_{2L}^2(13.6\text{ eV})]$, and g is a velocity-dependent correction term. They have used this form for both electron capture and ionization. In neither case does the g depend on the charge of the projectile Z_1. This expression predicts a linear dependence on Z_1 but does not extrapolate properly to the united atom limit.[25] The maximum binding correction would be the case where the L-shell electrons see a united atom (target plus projectile) potential. This corresponds to a correction factor of the form $\epsilon \approx (1 + (U_{ua} - U_B)/U_B)$.

The expressions used for ϵ in fitting the data are

$$\epsilon = 1 + aZ_1 + bZ_1^2 \tag{8}$$

or

$$\epsilon = 1 + (aZ_1 + bZ_1^2)g(V), \tag{9}$$

where the second form includes the velocity-dependent correction $g(V)$ taken from Eq. (19), Ref. 23. Figure 6 depicts the best fit of the data to various scaling laws. These plots have scaled the different sets of data so that they may be plotted with a single universal ionization curve.

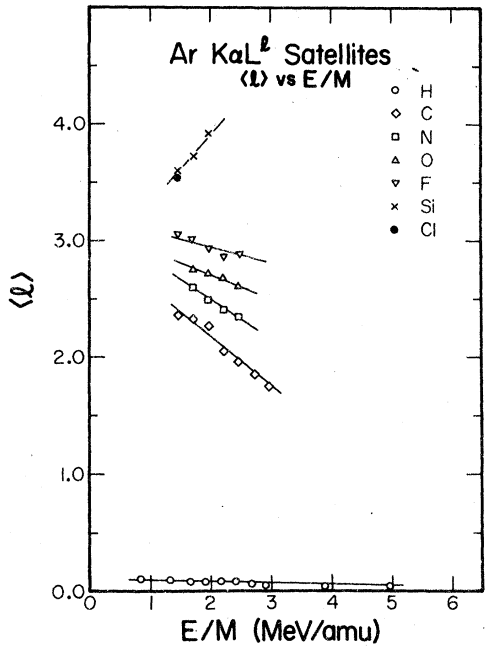

FIG. 4. Measured argon $K\alpha\ L^l$ average satellite number $\langle l \rangle$ plotted vs velocity squared (in MeV/amu). The lines are to guide the eye.

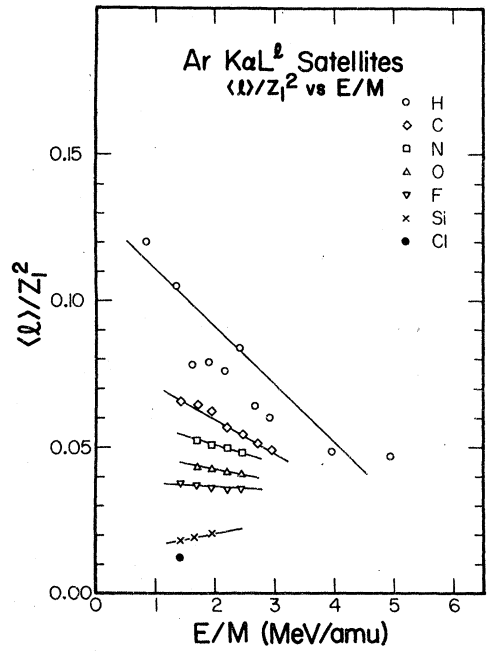

FIG. 5. Measured argon $K\alpha\ L^l$ average satellite number $\langle l \rangle$ with simple scaling with atomic number of the projectiles. The lines are to guide the eye.

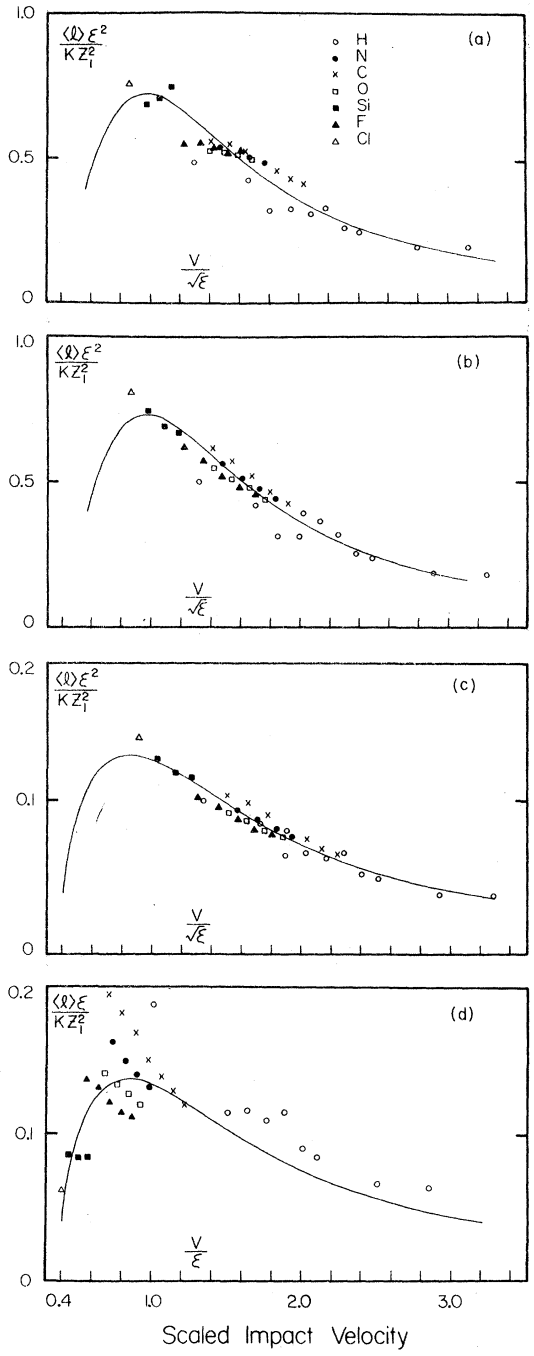

FIG. 6. Scaled measured average satellite number for Ar and theoretical universal ionization curves plotted vs scaled projectile velocity. Plot (a) uses a BEA universal ionization function, the BEA form for projectile scaling and no velocity dependence of the binding correction ϵ in the scaling adjustment. Plot (b) is the same as plot (a) except the velocity dependence of the binding correction is used in the scaling adjustment. Plot (c) is the same as plot (b) except the PWBA universal ionization function is used. Plot (d) is the same as plot (c) except the PWBA form for projectile scaling is used.

The data scaling corresponding to Eq. (7) is

$$\langle l\rangle \epsilon^{\nu}/KZ_1^2, \tag{10}$$

and the data was plotted versus $V\epsilon^{-\mu}$. Figure 6(a) and 6(b) show the improvement in the fit when the velocity-dependent correction is included in the expression for ϵ. The major effect seen is that the slopes of the individual projectile curves follow much more closely the theoretical ionization curve. Equation (9) was adopted as the better parameterization of the binding energy correction, and was used in the fits given in Fig. 6(c) and 6(d).

The results of fits of the $\langle l\rangle$ to the scaled ionization curves have indicated that the ionization curve predicted by the PWBA theory is slightly better than the analytical ionization curve obtained from the BEA theory. The criterion used in these tests is that a significantly lower reduced chi-squared value in the fit indicated a better approximation.

The BEA scaling [$\mu=0.5$ and $\nu=2$ in Eqs. (7) and (10)] yielded much better fits than the PWBA scaling [$\mu=\nu=1$ in Eqs. (7) and (10)] as can be seen in Fig. 6(c) and 6(d). Table III lists the values of the binding correction factor ϵ obtained from least-squares adjustments to the PWBA and BEA ionization curves. It also lists the values of ϵ predicted by the simple united atom model. As expected the fit values in columns 3 and 4 are smaller than the united atom values. Table IV lists the model parameters obtained from the adjustments.

B. Rearrangement analysis

The second method of analyzing the data involves using the energy shifts of the satellites to estimate

TABLE III. Binding-energy correction factors.

Z	E/A	Fit to BEA curve BEA scaling	Fit to PWBA curve BEA scaling	Fit to PWBA curve PWBA scaling	United atom estimates
1	0.85	1.08	1.03	1.36	1.18
1	1.38	1.06	1.03	1.29	1.18
1	1.64	1.06	1.02	1.27	1.18
1	1.90	1.05	1.02	1.25	1.18
1	2.16	1.05	1.02	1.24	1.18
1	2.41	1.05	1.02	1.22	1.18
1	2.67	1.05	1.02	1.21	1.18
1	2.92	1.04	1.02	1.20	1.18
1	3.94	1.04	1.02	1.18	1.18
1	4.95	1.03	1.01	1.16	1.18
6	1.44	1.61	1.41	2.54	2.29
6	1.70	1.57	1.38	2.42	2.29
6	1.95	1.52	1.36	2.34	2.29
6	2.20	1.50	1.34	2.27	2.29
6	2.46	1.48	1.32	2.20	2.29
6	2.71	1.46	1.31	2.15	2.29
6	2.96	1.44	1.30	2.10	2.29
7	1.70	1.72	1.50	2.63	2.55
7	1.95	1.67	1.47	2.53	2.55
7	2.20	1.64	1.45	2.45	2.55
7	2.46	1.60	1.43	2.37	2.55
8	1.70	1.88	1.64	2.82	2.82
8	1.95	1.82	1.60	2.71	2.82
8	2.20	1.78	1.57	2.62	2.82
8	2.46	1.74	1.54	2.53	2.82
9	1.44	2.14	1.86	3.16	3.10
9	1.70	2.06	1.79	3.00	3.10
9	1.95	1.99	1.75	2.88	3.10
9	2.20	1.94	1.71	2.78	3.10
9	2.46	1.89	1.67	2.69	3.10
14	1.44	3.34	2.94	3.98	4.82
14	1.70	3.17	2.80	3.76	4.82
14	1.95	3.04	2.69	3.59	4.82
17	1.44	4.26	3.81	4.34	6.13

TABLE IV. Universal scaling parameters for Ar+Z_1 collisions. Values a and b are from Eq. (9); K is from Eq. (10).

	BEA curve BEA scaling [a]	PWBA curve BEA scaling	PWBA curve PWBA scaling
a	0.31(10)	0.10(6)	1.68 (3)
b	0.047(6)	0.05(4)	−0.032(2)
K	0.28 (2)	1.19(5)	0.86 (3)
χ^2/n	0.38	0.23	1.9

[a]The numbers in parentheses are the fitting errors in the last digit.

the average number of M-shell vacancies $\langle m\rangle$ and comparing that number and the $\langle l\rangle$ to the results of a model calculation that includes rearrangement and vacancy-dependent transition rates as discussed in Sec. III. Figure 7 shows the variation of satellite position as a function of the projectile's nuclear charge. Since no significant projectile energy dependence is seen in the satellite position, the satellite channel numbers were averaged over projectile energy. The lines are the linear functions used to extrapolate the data to a charge of zero. To estimate the average number of M-shell vacancies the energy shifts of the satellites were compared to the theoretical results of Bhalla.[14] The energy shifts were estimated as the difference between the value of the fitted line at a particular Z and the value extrapolated to $Z=0$.

Table II shows the results of the analysis with and without rearrangement. The fourth and fifth columns are the results for P_L and P_M, respectively, from fitting the $\langle l\rangle$ and $\langle m\rangle$ experimental values to the model which includes rearrangement and vacancy-dependent decay rates. The last two columns are based on the same model with no rearrangement included but with the inclusion of vacancy-dependent rates. The latter P_L values thus differ from the $\frac{1}{8}\langle l\rangle$ values given in the third column only by the inclusion of the vacancy-dependent rates. The $\langle m\rangle$ values are not tabulated for the purpose of brevity and furthermore the $\frac{1}{8}\langle m\rangle$ values, obtained from the $K\alpha L^l$ energy shifts, are equal to the tabulated P_M values within the experimental uncertainties.

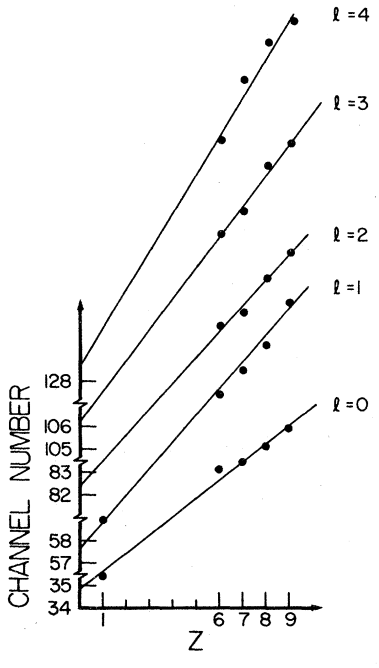

FIG. 7. Average satellite positions, in channel numbers, as a function of projectile atomic numbers. The channel number values may be converted to wavelength or energy by use of Table I (B). The solid lines are straight-line least-squares fits to the data.

V. CONCLUSION

The results presented here represent a large amount of experimental data on the projectile energy and atomic-number dependence of the $K\alpha$ satellite spectra of argon. The research was undertaken with the purpose of studying two effects: (i) the gas-solid differences in satellite spectra and (ii) the effect of M-shell rearrangement in a free-atom collision system. These two effects are not completely distinct since part of the gas-solid difference[8] or the light-ligand-gas–heavy-ligand-gas difference[10] is due to rearrangement. For the lower-Z-gas data there is also the projectile charge-state effect[6] which to date has not been observed in solids. For the Ar free-atom–gas case the rearrangement is not compli-

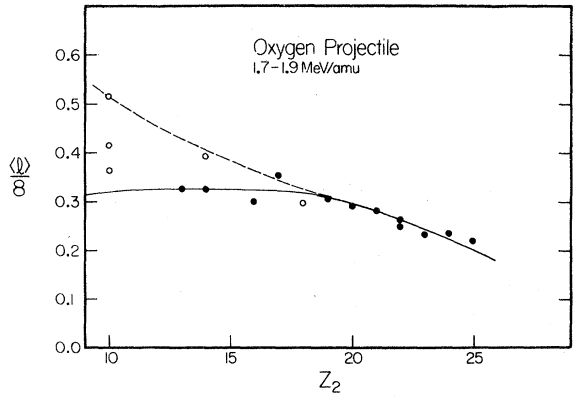

FIG. 8. Survey of $\frac{1}{8}\langle l\rangle$ for 1.7–1.9-MeV/amu oxygen on Ca-Mn, Ref. 28; Ti, Ref. 30; Al, Ref. 29; Si and S, Refs. 9 and 26; Ne, Ref. 6; Al, Cl, and K, Ref. 27; Ar, present work. Open circles are gas target data, and closed circles are solid target data.

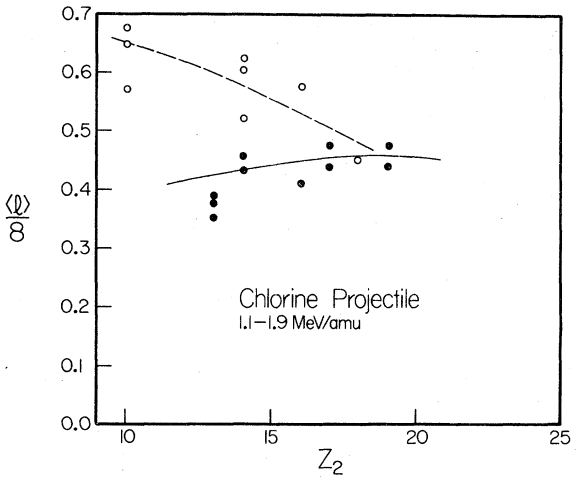

FIG. 9. Gas-solid effect on $\frac{1}{8}\langle l\rangle$ for 1.1–1.7-MeV/amu Cl on Ne, Ref. 6; Al, Ref. 29; Si, Refs. 10 and 31; S, Ref. 26; Cl and K, Ref. 27; two points for both targets are for S and Ar beams, and Ar present work. Open circles are gas target data and closed circles are solid target data.

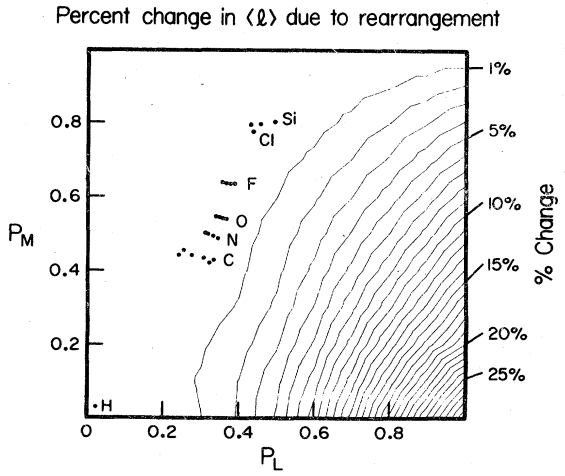

FIG. 10. Contour plots of percent change in the average $K\alpha L^l$ satellite number $\langle l\rangle$ due to outer-electron rearrangement as a function of the one-electron vacancy-production probabilities for the L shell, P_L, and the M shell, P_M. The points are the values of P_L and P_M obtained from the measured $\langle l\rangle$. Note that this model calculation predicts very little effect of rearrangement at the measured values.

cated by interatomic transitions.

The $K\alpha L^l$ satellite data from Ar yields $\langle l\rangle$ values which are systematically consistent with the values obtained from solid targets. This can be seen for oxygen projectiles in the 1.7–1.9-MeV/amu range in Fig. 8 which compares existing data[6,8,9,26-30] from Z_2 of 10 to 25. A solid-gas effect is observed for Z_2=14. At lower Z (Z=10) a large variation in $\langle l\rangle$ is observed as a function of projectile charge state. Similar systematics are observed for Cl projectiles[6,8,10,26,27,29] in the 1.1–1.9-MeV/amu range from Z_2 of 10 to 18 as shown in Fig. 9. Even though there is a large spread in the $\frac{1}{8}\langle l\rangle$ values, the gas-solid effect is very evident. The heavy-ligand-gas value of $\frac{1}{8}\langle l\rangle$ is seen to be nearly the same as the solid for Z_2 =16. The charge-state effect is also larger for the heavier projectile presumably due to the increase in the electron capture cross section with Z_1. From these systematics it is evident that the effect of rearrangement and the gas-solid effect are small for a target with as high an atomic number as argon. The charge-state effect may, however, reoccur at high Cl energies in which higher projectile charge states are reached.

The Ar data when analyzed with the rearrangement model shows virtually no L-shell filling due to M-shell electrons. In order to understand why rearrangement was not important for any of the projectiles a contour plot was made of the percent change in the predicted $\langle l\rangle$ due to rearrangement. Figure 10 shows that plot together with the reduced data obtained from the fits. It is seen that all the data points lie below the 1% contour. This is a result of the fact that in none of the cases were large numbers of L-shell vacancies produced without also producing large numbers of M-shell vacancies. Rearrangement may become important at higher projectile energies where P_L may be larger than P_M.

The attempt to fit the experimental $\langle l\rangle$ values to a universal curve is justified by the result that rearrangement and vacancy-dependent rates had very little effect on the fitted value of $P_L(0)$ when compared to the simple theory, i.e., $\frac{1}{8}\langle l\rangle$.

The most important result of this work is the demonstration of a universal behavior of $\langle l\rangle$ obtained from the single-K- multiple-L-shell satellite spectra of Ar. The quantity $\langle l\rangle\epsilon^2/KZ_1^2$ vs $V/\sqrt{\epsilon}$ agrees very well with the PWBA ionization function for K=1.19 and $\epsilon=1+(0.1Z_1+0.05Z_1^2)g(V)$ and nearly as well with the BEA ionization function for K=0.28 and $\epsilon=1+(0.31Z_1+0.047Z_1^2)g(V)$. This function can thus be used to predict multiple ionization over a large range of incident energy and projectile Z for elements near Ar. Additional systematic measurements of $\langle l\rangle$ for solid targets would serve as a test of the proposed function and would also give insight into the Z_2 dependence of K.

ACKNOWLEDGMENT

This work was supported in part by the Division of Chemical Sciences, U.S. Department of Energy.

[1]A. R. Knudson, D. J. Nagel, P. G. Burkhalter, and K. L. Dunning, Phys. Rev. Lett. 26, 1149 (1971).
[2]D. Burch, P. Richard, and R. L. Blake, Phys. Rev. Lett. 26, 1355 (1971).
[3]R. L. Watson, T. Chiao, and F. E. Jenson, Phys. Rev. Lett. 35, 254 (1975).
[4]C. F. Moore, D. L. Matthews, and H. H. Wolter, Phys. Lett. A 54, 407 (1975).
[5]F. Hopkins, J. Sokolov, and A. Little, Phys. Rev. A 14, 1907 (1976).
[6]R. L. Kauffman, C. W. Woods, K. A. Jamison, and P. Richard, Phys. Rev. A 11, 872 (1975).
[7]D. L. Matthews, C. F. Moore, and D. Schneider, Phys. Lett. A 48, 27 (1974).
[8]R. L. Kauffman, K. A. Jamison, T. J. Gray, and P. Richard, Phys. Rev. Lett. 36, 1074 (1976).
[9]R. L. Watson, A. K. Leeper, B. I. Sonobe, T. Chaio, and F. E. Jenson, Phys. Rev. A 15, 914 (1977).
[10]F. Hopkins, A. Little, N. Cue, and V. Dutkiewicz, Phys. Rev. Lett. 37, 1100 (1976).
[11]M. H. Chen and B. Crasemann, Phys. Rev. A 12, 959 (1975).
[12]C. P. Bhalla, N. O. Folland, and M. A. Hein, Phys. Rev. A 8, 649 (1973).
[13]M. H. Chen and B. Crasemann, Phys. Rev. A 10, 2232 (1974).
[14]C. P. Bhalla, Phys. Rev. A 8, 2877 (1973).
[15]E. J. McGuire, Phys. Rev. A 3, 587 (1971).
[16]J. M. Hansteen, O. M. Johnsen, and L. Kocbach, At. Data Nucl. Data Tables 15, 305 (1975).
[17]G. S. Khandelwal, B. H. Choi, and E. Merzbacher, At. Data 1, 103 (1969).
[18]J. H. McGuire and P. Richard, Phys. Rev. A 8, 1374 (1973).
[19]B. H. Choi, E. Merzbacher, and G. S. Khandelwal, At. Data 5, 291 (1973).
[20]E. J. McGuire, Phys. Rev. A 3, 587 (1971).
[21]E. P. Larkins, J. Phys. B 4, L29 (1971).
[22]G. Basbas, W. Brandt, and R. Laubert, Phys. Rev. A 7, 983 (1973).
[23]W. Brandt and G. Lapicki, Phys. Rev. A 10, 474 (1974).
[24]G. Lapicki and W. Losonsky, Phys. Rev. A 15, 896 (1977).
[25]R. Anholt and W. E. Meyerhof, Phys. Rev. A 16, 190 (1977).
[26]J. A. Demarest and R. L. Watson, Progress Report: Cyclotron Institute, Texas A & M University (1977), p. 72.
[27]R. L. Watson, F. E. Jensen, and T. Chaio, Phys. Rev. A 10, 1230 (1974).
[28]R. L. Kauffman, J. H. McGuire, P. Richard, and C. F. Moore, Phys. Rev. A 8, 1233 (1973).
[29]F. Hopkins, D. O. Elliott, C. P. Bhalla, and P. Richard, Phys. Rev. A 8, 2952 (1973).
[30]K. W. Hill, B. L. Doyle, S. M. Shafroth, D. H. Madison, and R. D. Deslattes, Phys. Rev. A 13, 1334 (1976).